UNIVERSIDAD DE SANTIAGO DE CHILE

FACULTAD DE CIENCIA

Departamento de Física

Entangled photon generation with metal-organic frameworks

Simón Joaquín Paiva Ortega

Profesor Guía:

Felipe Herrera Urbina

Tesis presentada en el cumplimiento de los requisitos para la obtención del grado de:

Magíster en Ciencias con mención en Física

Santiago – Chile

2022

Contents

Chapter 1

Introduction

Spontaneous Parametric Down-Conversion (SPDC) is a non-linear optical process that serves as the basis for many quantum optics experiments, such as one-photon interference, biphoton interference, polarization and interference [1], quantum cryptography [2], quantum simulation [3] and, quantum metrology [4]. In SPDC one photon of frequency ω is converted spontaneously into two photons at frequencies ω_1 and ω_2, which due to energy conservation satisfy $\omega = \omega_1 + \omega_2$. Down-conversion is typically inefficient, with only a small fraction of photons converted in a non-linear crystal. Among the usual crystals used to do experimental SPDC are KDP and BBO [5], but there are novel materials that are noncentrosymmetric that have not been studied for quantum optics yet. One of these new material classes is the metal-organic frameworks (MOF), which can be tailor-designed to be noncentrosymmetric and transparent in visible light, for quantum optics applications.

1.1 Quantum entanglement and Bell states

A bipartite pure quantum state is called entangled when it can not be written as two separate states, and the quantum state is a superposition of the two pure states [6].

Consider a pure state for a system composed of two spatially separated subsystems,

$$\hat{\rho} = |\Psi\rangle\langle\Psi|, \qquad |\Psi\rangle = \sum_{a,b} c(a,b)|a\rangle|b\rangle \tag{1.1}$$

where $\hat{\rho}$ is the density matrix, $|a\rangle$ and $|b\rangle$ are quantum states for the two subsystems. If $c(a,b)$ is such that the two particles state $|\Psi\rangle$ factor into a product of wave functions for the two subsystems therefore

$$|\Psi\rangle = |\Psi_a\rangle|\Psi_b\rangle, \tag{1.2}$$

we say that the two subsystems are entangled.

One type of two-particle entanglement was proposed by Einstein, Podolsky and Rosen (EPR) to be of the form,

$$|\Psi\rangle = \sum_{a,b} \delta(a + b + c_0)|a\rangle|b\rangle \tag{1.3}$$

where a and b correspond to the momentum of each particle and c_0 is a constant. For this type of entangled state, the value of the momentum or the position of one particle is undetermined for a single individual system. However, if one of the subsystems is measured at a certain value then the other subsystem also acquires a well-defined momentum. This property was called by EPR as "spooky action at a distance" [7].

There are several types of entangled quantum states. For this thesis, we focus on polarization entangled states. Bell states are well-known two particles entangled states, as they occur naturally for polarization states of entangled photon pairs produced in SPDC [8, 9, 10]. They are four Bell states which form a complete orthonormal basis and are represented by

$$|\Phi^{\pm}_{12}\rangle = \frac{1}{\sqrt{2}}[|0_1 0_2\rangle \pm |1_1 1_2\rangle], \quad |\psi^{\pm}_{12}\rangle = \frac{1}{\sqrt{2}}[|0_1 1_2\rangle \pm |1_1 0_2\rangle], \tag{1.4}$$

Here the basis $|0\rangle$ and $|1\rangle$ represent two orthonormal polarization basis, for example, if $|0\rangle$ is $|V\rangle$ (vertical polarization), $|1\rangle$ is $|H\rangle$ (horizontal polarization). To prepare Bell states experimentally, it is necessary to make the wavepackets overlap in space and time, which makes the quantum mechanically indistinguishable from each photon subsystem.

This theory to represent entangled quantum states is not amenable to experiments, because this is convenient to introduce a Bell inequality that is based on the Bell states, and show that the nature cannot be described by local hidden-variables theory, this inequality can be introduced as follows: Alice and Bob are in two separate locations. A third actor called Mallory prepares a pair of entangled particles and sends one to Bob and the other to Alice. When Bob receives the particle he decides to perform one of two possible measurements. Consider both measurements as binary, this means the measure can only be $+1$ or -1 if we denote this measure of Bob like A_0 and A_1. The same procedure for Bob´s particle but with a denote measure of B_0 and B_1, also binary.

If Bob chooses to measure A_0 and get $+1$, then the particle he received has a value of $+1$ in a property a_0. Considering the following expression

$$a_0 b_0 + a_1 b_0 + a_0 b_1 - a_1 b_1 = b_0(a_0 + a_1) + b_1(a_0 - a_1) \tag{1.5}$$

Because a_0 and a_1 from the Eq. (1.5) take values of ± 1, either the $(a_0 + a_1)$ is zero or $(a_0 - a_1)$ is zero, then one of the two terms will vanish and the other will have a value of ± 2. If we do the same experiment over and over again, with Mallory preparing new pairs of particles for each experiment, then the average value of the combination of the left-hand side of the Eq. (1.5) across all the experiments will be equal or less than 2. The expression for this inequality is the following, considering angle brackets as the average values

$$\langle A_0 B_0 \rangle + \langle A_1 B_0 \rangle + \langle A_0 B_1 \rangle - \langle A_1 B_1 \rangle \leqslant 2 \tag{1.6}$$

The Eq. (1.6) is called the Bell inequality, more specifically, the CHSH inequality [11]. This derivation has two assumptions, first that the underlying physical properties $a_0, a_1, b_0, a_0, a_1, b_0$, and $b_1 b_1$ exist independently of being observed or measured, this is also called the assumption of realism, and the second assumption is that Bob's action cannot influence Alice's results or measurement and vice versa, this is also called the assumption of locality. Violating this inequality implies that the particle that Alice and Bob receive are entangled.

Some applications of entangled particles are quantum cryptography [12, 13, 14], quantum imaging, more specifically ghost imaging [15, 16, 17, 18, 19], quantum teleportation [20, 21, 22], among others.

1.2 Optics of uniaxial crystals

Crystals can be classified by the types of symmetry elements that can support their lattice structure. The most basic symmetry element is the inversion, which transforms (x, y, z) coordinates to $(-x, -y, -z)$ [23]. Crystals whose unit cells are invariant under inversion are said to not have inversion symmetry or are called non-centrosymmetric. Chiral crystals do not have an inversion symmetry. Several crystal classes are non-centrosymmetric (no inversion symmetry).

Typically for a centrosymmetric crystal, the leading contributor for the nonlinear polarization is the $\chi^{(3)}$ third-order susceptibility tensor, but for a non-centrosymmetric crystal we can expand the polarization and therefore we have contributions of more orders of the susceptibility tensors where $\chi^{(2)}$ is the second-order susceptibility tensor.

Uniaxial crystals are noncentrosymmetric. They have at least one non-zero component of the $\chi^{(2)}$ tensor, also have one axis, called optical axis (OA) or extraordinary axis, with a distinct value of the refractive index, and two crystal axis having the same index, which is called the ordinary axes.

For uniaxial crystals the $\chi^{(1)}$ susceptibility tensor is

$$\chi^{(1)} = \begin{pmatrix} n_o & 0 & 0 \\ 0 & n_o & 0 \\ 0 & 0 & n_e \end{pmatrix} \tag{1.7}$$

where we take into consideration that the extraordinary axis is in the z coordinate. Some of the crystal classes for uniaxial crystals are tetragonal, trigonal and hexagonal [24].

Depending on the relative values of n_o and n_e, we can have two types of uniaxial crystals, a positive uniaxial crystal correspond to a crystal that has a higher value of the extraordinary refractive index n_e than the ordinary refractive index n_o, for example, the Quartz is a positive uniaxial crystal. The negative corresponds to uniaxial crystals that have a lower value of the n_e than n_o. Beta-barium borate (BBO) is a well-known negative uniaxial crystal.

The refractive index of uniaxial crystals (positive and negative) can be described as a function of wavelength using the Sellmeier equation. This equation is used to determinate the light dispersion response in the medium. For BBO the corresponding Sellmeier equation reads, this equation is valid in the range of $\lambda_{min} = 220\text{nm}$ to $\lambda_{max} = 1060\text{nm}$ [25]

$$n_o^2 = 2.7405 + \frac{0.0184}{\lambda^2 - 0.0179} - 0.0155\lambda^2 \quad \text{and} \quad n_e^2 = 2.3730 + \frac{0.0128}{\lambda^2 - 0.0156} - 0.0044\lambda^2 \tag{1.8}$$

we have another example, the Sellmeier equations for Quartz, are in the range of $\lambda_{min} = 198\text{nm}$ to $\lambda_{max} = 2050\text{nm}$ [26], are given by

$$\begin{aligned} n_o^2 &= 1.28604141 + \frac{1.07044083\lambda^2}{\lambda^2 - 1.00585997 \times 10^{-2}} - \frac{1.10202242\lambda^2}{\lambda^2 - 100} \\ n_e^2 &= 1.28851804 + \frac{1.09509924\lambda^2}{\lambda^2 - 1.02101864 \times 10^{-2}} - \frac{1.15662475\lambda^2}{\lambda^2 - 100} \end{aligned} \tag{1.9}$$

In Fig.1.1 we show the Sellmeier curves for (a) BBO and (b) Quartz, obtained from Eqs.(1.8) and (1.9), respectively.

Another non-centrosymmetric crystal of interest is the biaxial crystal, that has three different refractive indexes. If we take into consideration a plane that only contains two of the three axes of a biaxial crystal, we only gonna have the contributions of two refractive indexes therefore approach a biaxial crystal into a uniaxial one, this can be done for every biaxial crystal, and will be usefull later in this Thesis. Some of the crystal classes that are biaxial crystals are Orthorhombic, Monoclinic and Triclinic.

Inorganic crystals are typically used for non-linear optics, such as KH_2PO_4 (KDP) or BaB_2O_4 (BBO), because they have large second-order non-linear susceptibility and optical anisotropy in the visible spectrum and near-infrared, which is exploited for SPDC.

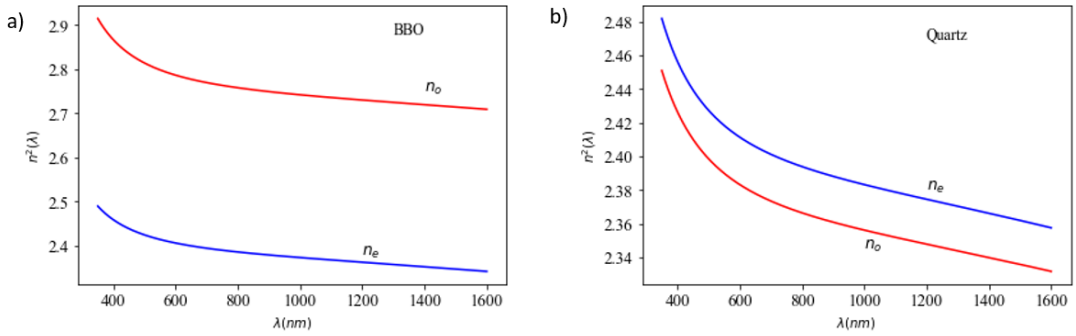

Figure 1.1: (a) Sellmeier equation for BBO (negative uniaxial), (b) Sellmeier equation for Quartz (positive uniaxial), where the red line corresponds to the ordinary refractive index and the blue line correspond to the extraordinary refractive index

1.3 Metal-Organic Frameworks

Metal-Organic Frameworks (MOFs) are crystalline materials composed of a metallic center and organic ligands, and can be tailor-designed based on the way that the ligands and the center self-assemble. MOF crystals are very promising for applications in nonlinear optics, this is due to the great number of MOFs that are non-centrosymmetric and show promising optical response [27].

There are currently more than 88.000 MOF structures in the Cambridge Structural Database [28]. There are two main categories for MOF crystals, porous crystals, and nonporous crystals. There are 29.4% porous MOFs and 70.6% nonporous MOFs in the literature [29]. This is relevant because the main uses for the industry are gas storage and gas separation, which are related properties to the pore size of the lattice. Fig. 1.2 shows the difference between the two types of MOFs where (a) is a non-porous crystal and (b) corresponds to a highly porous crystal. Typically the nonporous MOFs are not very noticeable but for nonlinear optics, the porosity does not matter, this leads us to have a huge potential in optics because many MOFs crystals nonporous were available in the structural databases. Recent experimental reports have shown competitive values for second-order [30] and third-order [31] nonlinear properties for polycrystalline MOF crystals. Due to this high potential in nonlinear properties such as second-order nonlinearity, the great number of neglected crystals for nonporous crystals, and the tailor-based design, the MOFs are the perfect new scope to research in nonlinear optics crystals.

Large-scale computational MOF screening methods for applications in gas storage and gas separation have been developed, and extensions to these techniques can be developed to discover novel applications for MOFs in quantum technology, due to the potential nonlinearity of these crystals.

For this work, we focus on selected MOFs that are noncentrosymmetric and transparent thought out the visible spectrum. To characterize this crystal in non-linear optics we need the Sellmeier equations and the $\chi^{(2)}$ tensor. The selected MOFs are MIRO-101, MIRO-102, and MIRO-103, which have been

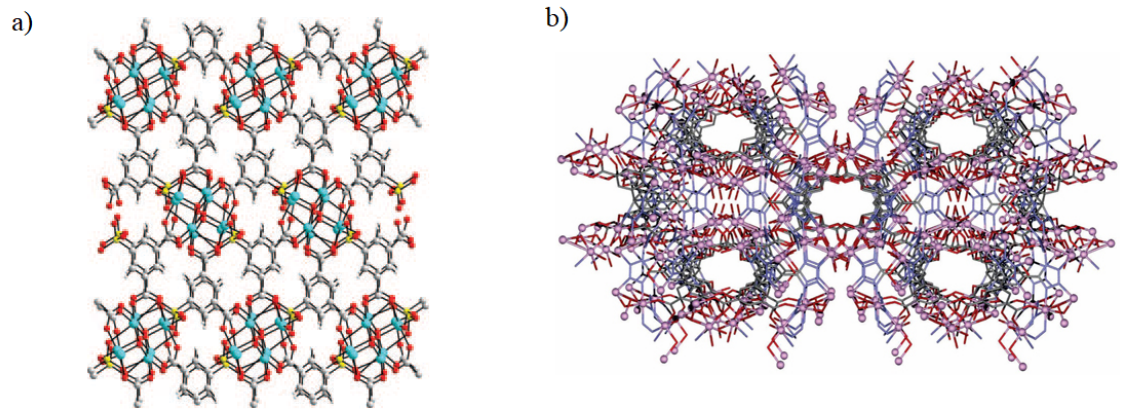

Figure 1.2: (a) Nonporous MOF $Cu_2(OH)(C_8H_3O_7S)(H_2O) \cdot 2H_20$, adapted from Ref. [32] and (b) porous MOF CRISPR/Cas9 adapted from Ref. [33].

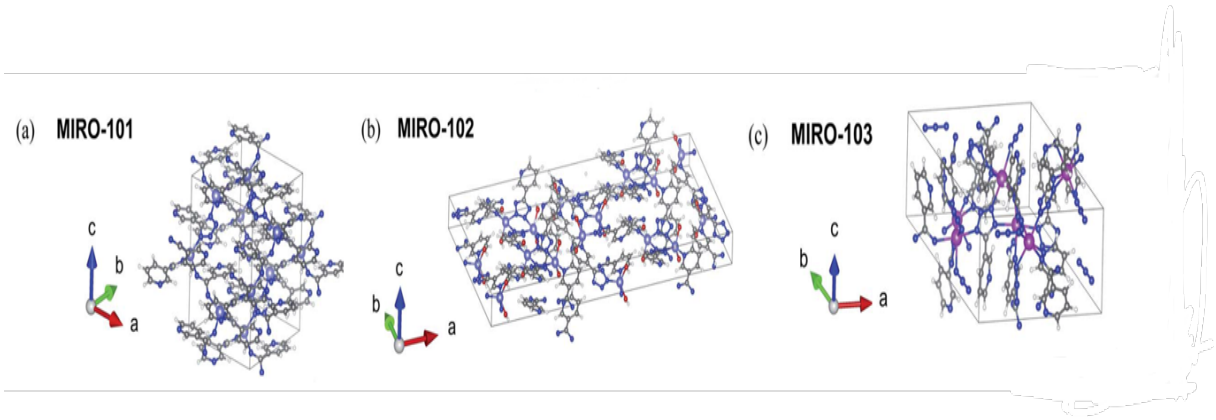

Figure 1.3: Examples of MOFs with a core of Zn_2, (a) correspond to the MIRO-101,(b) correspond to the MIRO-102, and (c) correspond to the MIRO-103 [27].

studied before for other phase matching conditions in Ref.[34].

1.4 State of the Art

SPDC phenomena have different applications for entangled-photons, such as quantum teleportation [35], quantum computing [36], quantum communication [37], quantum cloning [38], quantum cryptography [39], polarization [40], optical imaging using entanglement photons [41], quantum spectroscopy [42] and Optical lithography [43] among other.

Typically these experimental applications use the same type of crystals, including lithium niobate, BBO, and KDP among others. In more recent years quasi-phase matched waveguide crystals are being used to achieve higher SPDC efficiency, although, in a restricted phase-matching range such as

a PPKTP, that is a periodically-poled waveguide crystal based on the KTP crystal [44].

The scope of new crystals for entangled photons is not in organic-based crystals such as MOFs, the objective of this thesis is to enlarge this scope to target this new tailor-based design organic crystals, to do so a comparison between experimentally used crystals and new MOFs crystals with non-centrosymmetric symmetry is necessary and is provided in this works.

Chapter 2

Spontaneous Parametric Down-Conversion (SPDC)

2.1 Fundamentals of SPDC

In a non-linear crystal, for instance, a uniaxial o biaxial crystal, that is pumped by an intense laser beam at frequency ω_p, two weak fields, called signal and idler, are produced at frequency ω_s and ω_i, respectively such that $\omega_p = \omega_i + \omega_s$.

The quantum theory behind the SPDC can be derived from the classical description of non-linear interaction, followed by the quantization of the electromagnetic field. We expand to second order the electric polarization of a nonlinear and noncentrosymmetric optical medium gives us

$$P_i(r,t) = \epsilon_0 \int_0^\infty dt^{'} \chi_{\text{ij}}^{(1)}(t') E_j(r, t-t') + \int_0^\infty dt' \int_0^\infty dt'' \chi_{\text{ijk}}^{(2)}(t', t'') E_j(r, t-t') E_k(r, t-t'') \quad (2.1)$$

where $E_j(r,t)$ is the j component of the electric field vector that propagates in the medium and $\chi^{(1)}$ and $\chi^{(2)}$ are the first and second susceptibility tensors, respectively.

To quantize the electromagnetic field, start from, the electromagnetic field Hamiltonian in the dielectric medium of volume V, it is

$$\hat{\mathcal{H}}(t) = \frac{1}{2} \int_V dr [\mathbf{D}(r,t) \cdot \mathbf{E}(r,t) + \mathbf{B}(r,t) + \mathbf{H}(r,t)] \quad (2.2)$$

where **D** is the displacement field vector, **B** the magnetic induction and **H** is the magnetic field. Now we can use the definition of the displacement field $\mathbf{D}(r,t) = \epsilon_0 \mathbf{E}(r,t) + \mathbf{P}(r,t)$, to rewrite the Eq. (2.2), and the Eq. (2.1) we obtain

$$\hat{\mathcal{H}}(t) = \hat{\mathcal{H}}_0(t) + \hat{\mathcal{H}}_I(t) \quad (2.3)$$

In this case, the first term corresponds to the linear interaction of the electric polarization and the second term is a nonlinear perturbation, given by

$$\hat{\mathcal{H}}_I(t) = \frac{1}{2}\int_V dr \int_0^\infty dt' \int_0^\infty dt'' E_i(\mathbf{r},t)\chi^{(2)}_{ijk}(t',t'')E_j(\mathbf{r},t-t')E_k(\mathbf{r},t-t'') \tag{2.4}$$

note that we are using the Einstein summation convention to simplify notation. Now we can expand the classical optical electric field in terms of planes waves as

$$\mathbf{E}(r,t) = \mathbf{E}^{(+)}(r,t) + \mathbf{E}^{(-)}(\mathbf{r},t) \tag{2.5}$$

where

$$\mathbf{E}^{(+)}(\mathbf{r},t) = \frac{1}{\sqrt{V}}\sum_{\mathbf{k},\sigma} e_{\mathbf{k},\sigma}\epsilon_{\mathbf{k},\sigma}\alpha_{\mathbf{k},\sigma}G(\omega)exp[i(\mathbf{k}\cdot\mathbf{r}-\omega t)] = [\mathbf{E}^{(-)}(\mathbf{k},t)]^* \tag{2.6}$$

is the field expansion, with

$$\epsilon_{\mathbf{k},\sigma} = \sqrt{\hbar\omega(\mathbf{k},\sigma)/2\epsilon_0 n^2(\mathbf{k},\omega)} \tag{2.7}$$

where the index σ is summed over a two-dimensional orthogonal polarization vector. ϵ_0 is the free space permittivity, $G(\omega)$ is a transmission function that models the detector filter, V is the quantization volume, $\mathbf{k}$ is an index summed over all wave vectors, $e_{\mathbf{k},\sigma}$ is the two-dimensional unit polarization vector, ω the frequency and $\alpha_{\mathbf{k},\sigma}$ is the mode amplitude. We adopt the usual method of quantization for the electric field, substituting the amplitude coefficient $\alpha_{\mathbf{k},\sigma}$ for the photon annihilation operator $\hat{a}_{\mathbf{k},\sigma}$.

Substituting Eq. (2.6) into the classical Hamiltonian Eq. (2.4) we have a quantum Hamiltonian operator

$$\hat{\mathcal{H}}_I = \frac{1}{2\nu^{3/2}}\sum_{\mathbf{k}_s,\sigma_s}\sum_{\mathbf{k}_p,\sigma_p}\sum_{\mathbf{k}_i,\sigma_i} g^*_{\mathbf{k}_s,\sigma_s}g^*_{\mathbf{k}_i,\sigma_i}g^*_{\mathbf{k}_p,\sigma_p}a^\dagger_{\mathbf{k}_s,\sigma_s}a^\dagger_{\mathbf{k}_i,\sigma_i}a_{\mathbf{k}_p,\sigma_p}\ \ exp[i(\omega_s+\omega_i-\omega_p)t]$$

$$\times\ \ \chi_{ijk}(\mathbf{e}_{\mathbf{k}_s,\sigma_s})^*_i(\mathbf{e}_{\mathbf{k}_i,\sigma_i})^*_j(\mathbf{e}_{\mathbf{k}_p,\sigma_p})_k\int_V e^{[-i(\mathbf{k}_s+\mathbf{k}_i-\mathbf{k}_p)\cdot\mathbf{r}]}\ \ dr + H.C. \tag{2.8}$$

where s, i, p correspond to the signal, idler, and pump field respectively.

$$g_{\mathbf{k},\sigma} = i\sqrt{\frac{\hbar\omega(\mathbf{k},\sigma)}{2\epsilon_0 n^2(\mathbf{k},\sigma)}}G[\omega(\mathbf{k},\sigma)] \tag{2.9}$$

V is the interaction volume and H.C. stands for the Hermitian conjugate, $n(\mathbf{k},\sigma)$ is the linear refractive index of the anisotropic crystal.

To obtain the quantum state produced by SPDC, we assume that the nonlinear interaction is turned on at time $t_0 = 0$ when the system is in the initial state $|\psi(0)\rangle$. The state at time t is given by the time evolution by

$$|\psi(t)\rangle = U(t)|\psi(0)\rangle \tag{2.10}$$

with the time evolution operator

$$U(t) = e^{\left(\frac{-i}{\hbar}\int_0^t dt H_I(\tau)\right)} \tag{2.11}$$

when the pump field is sufficiently weak, we can expand the evolution operator in power series, then we integrate over space the r that leads to a sinc function involving the wave vector, which provides the conservation of momentum

$$\begin{aligned}\int_0^t dt H_I(\tau)) &= \frac{Vt}{2\nu^{3/2}} \sum_{\mathbf{k}_s,\sigma_s} \sum_{\mathbf{k}_p,\sigma_p} \sum_{\mathbf{k}_i,\sigma_i} \mathbf{g}^*_{\mathbf{k}_s,\sigma_s} \mathbf{g}^*_{\mathbf{k}_i,\sigma_i} \mathbf{g}^*_{k_p,\sigma_p} \mathbf{a}^\dagger_{\mathbf{k}_s,\sigma_s} \mathbf{a}^\dagger_{\mathbf{k}_i,\sigma_i} \mathbf{a}_{\mathbf{k}_p,\sigma_p} \;\; e^{[i(\omega_s+\omega_i-\omega_p)t/2]} \\ &\times \quad \chi_{ijk}(\mathbf{e}_{\mathbf{k}_s,\sigma_s})^*_i (\mathbf{e}_{\mathbf{k}_i,\sigma_i})^*_j (\mathbf{e}_{\mathbf{k}_p,\sigma_p})_k \mathrm{sinc}[(\omega_s+\omega_i-\omega_p)t/2] \\ &\times \quad \prod_m \mathrm{sinc}[(\mathbf{k}_s+\mathbf{k}_i-\mathbf{k}_p)_m l_m/2] e^{[-i((\mathbf{k}_s+\mathbf{k}_i-\mathbf{k}_p)_z l_z/2]} + H.C. \end{aligned} \tag{2.12}$$

where $V = l_x \times l_y \times l_z$ and l_m is the dimension of the nonlinear medium in the direction $m = (x, y, z)$. For more details in the volume integral, see Appendix A.1.

Now we can finally derive an expression for the quantum state as time t, using Eq. (2.12) on Eq. (2.10) and considering the initial state as vacuum we obtained:

$$\begin{aligned}|\psi(t)\rangle = |vac\rangle + \frac{Vt}{2i\hbar\nu^{3/2}} &\sum_{\mathbf{k}_s,\sigma_s} \sum_{\mathbf{k}_p,\sigma_p} \sum_{\mathbf{k}_i,\sigma_i} \mathbf{g}^*_{\mathbf{k}_s,\sigma_s} \mathbf{g}^*_{\mathbf{k}_i,\sigma_i} \mathbf{g}^*_{\mathbf{k}_p,\sigma_p} \alpha_p(\mathbf{k}_p,\sigma_p) \;\; e^{[i(\omega_s+\omega_i-\omega_p)t/2]} \\ &\times \quad \chi_{ijk}(\mathbf{e}_{\mathbf{k}_s,\sigma_s})^*_i (\mathbf{e}_{\mathbf{k}_i,\sigma_i})^*_j (\mathbf{e}_{\mathbf{k}_p,\sigma_p})_k \mathrm{sinc}[(\omega_s+\omega_i-\omega_p)t/2] \\ &\times \prod_m \mathrm{sinc}[(\mathbf{k}_s+\mathbf{k}_i-\mathbf{k}_p)_m l_m/2] \;\; exp[-i((\mathbf{k}_s+\mathbf{k}_i-\mathbf{k}_p)_z l_z/2] |\mathbf{k}_s,\sigma_s\rangle |\mathbf{k}_i,\sigma_i\rangle \end{aligned} \tag{2.13}$$

where $|k_s,\sigma_s\rangle$ and $|k_i,\sigma_i\rangle$ denote the Fock states for the signal and idler respectively, and $\alpha_p(k_p,\sigma_p)$ is a classical amplitude corresponding to the plane wave component (k_p,σ_p) of the pump beam, that replace the annihilation operator for the pump modes. We simplify the equation (2.1), using the following approximations:

(a) The interaction time is long enough, so the sinc function for the frequencies are only relevant when $\omega_p = \omega_s + \omega_i$. The power of the pump laser is moderate so that the time interval between two down-conversion events is large compared to the detection time.

(b) The frequency spread of the detectable down-converted fields is small compared to the central frequencies so that the dispersion of the refractive indices around the central frequencies $\overline{\omega}_j$ is small and a linear approximation can be used. This assumption is justified by the use of narrow-band interference filters in front of the detectors.

(c) The terms g_{k_j,σ_j} and $\chi^{(2)}_{ijk}$ are slowly-varying functions of k_j, so they may be taken as constants in the intervals considered for k_j.

(d) The pump beam propagates along the z-axis and the crystal is large enough in the x and y directions to contain the whole pump beam transverse profile. In this case, l_x and l_y can be extended

to infinity, and the last term in the third line of expression (2.1) is proportional to

$$\delta(q_s + q_i - q_p)\mathrm{sinc}[(k_{sz} + k_{iz} - k_{pz})L/2] \tag{2.14}$$

where $q_j = (k_{jx}, k_{jy})$ is the transverse component of $\mathbf{k}_j$ and $L = l_z$ is the crystal propagation length (thickness).

(e) The quantization volume is large enough to justify the replacement of summations over k by integrals.

Under these assumptions, Eq. (2.1) is written as

$$|\psi\rangle = |vac\rangle + \sum_{\sigma_s,\sigma_i} \int d\omega_s \int d\omega_i \int dq_s \int dq_i \Phi_{\sigma_s,\sigma_i}(q_s, q_i, \omega_s, \omega_i)|q_s, \omega_s, \sigma_s\rangle|q_i, \omega_i, \sigma_i\rangle \tag{2.15}$$

where $|q_j, \omega_j, \sigma_j\rangle$ represents a one-photon state in the mode defined by the transverse component q_j of the wave vector, by the frequency ω_j and by the polarization σ_s. The amplitude Φ is given by

$$\Phi_{\sigma_s,\sigma_i} = C_{\sigma_s,\sigma_i} G_s G_i \alpha(q_s + q_i, \omega_s + \omega_i)\mathrm{sinc}[(k_s z + k_i z - k_p z)L/2] \tag{2.16}$$

where C_{σ_s,σ_i} is a coupling constant that depends on the nonlinear susceptibility tensor, and $G(\omega_j)$ is the spectral function defined by the narrow bandwidth filters placed in front of the detectors.

2.2 Phase matching

SPDC consists of the interaction of a nonlinear crystal with a photon that leads to the annihilation of this photon and the creation of two photons of lower energies, this procedure needs to satisfy energy and momentum conservation conditions, these conditions are

$$\omega_p = \omega_s + \omega_i, \qquad \mathbf{k}_p = \mathbf{k}_s + \mathbf{k}_i \tag{2.17}$$

where ω_j and k_j are the frequency and the wavevector of the photon j ($j = s, i, p$), respectively, the first equation is due to energy conservation, and the second is called the phase matching equation. Satisfying both Eq. (2.17) is known as perfect phase matching.

There are two types of SPDC, which differ from each other in the type of polarization that the SPDC phenomena generates, the first one is called SPDC Type I and have the property to generate two photons with the same polarization, and perpendicular polarization to the converted photon (photon that is converted in two photons via SPDC), otherwise the Type II SPDC has the property to generate two photons with perpendicular polarization to each other, and one of them have the same polarization that the converted photon. In this thesis, the center of the study will be SPDC Type II. The types of

	Type I	Type II
Negative	$e \Rightarrow o, o$	$e \Rightarrow o, e$
Positive	$o \Rightarrow e, e$	$o \Rightarrow o, e$

Table 2.1: Types of polarization for Type I and Type II SPDC, where the left-hand of the arrow corresponds to the converted photon and the two on the right hand of the arrow correspond to the generated photons, e is the extraordinary polarization and o is the ordinary polarization.

polarization are shown in the table 2.1.

For the two generated photons in SPDC type II, shown in table 2.1, the polarization can be switched between them, for instance, the o,e polarization in Type II SPDC positive can be switched as e,o and have the same physics.

2.2.1 Type II Phase matching: planar case

For this thesis, the focus will be on Type II SPDC for positive and negative uniaxial.

We consider type-II phase matching. The pump wavevector k_p makes an angle Ψ with the Optical Axis (OA) inside the crystal, as illustrated in Fig. (2.1). We are interested in how the output angles θ_e^o and θ_o^o change as a function of wavelength for a given OA angle Ψ. The vectorial wavevector condition $\Delta E = 0$ gives a system of equations for the components that read

$$\mathbf{k}_e \cos\theta_e + \mathbf{k}_o \cos\theta_o = \mathbf{k}_p. \tag{2.18}$$

$$\mathbf{k}_e \sin\theta_e = \mathbf{k}_o \sin\theta_o \tag{2.19}$$

where $\mathbf{k}_o$, $\mathbf{k}_e$, and $\mathbf{k}_p$ are the vectorial wavevector for the ordinary, extraordinary, and pump photon, respectively. θ_e and θ_o are the angles between the ordinary and extraordinary wavevector, and the normal to the plane of incidence of the pump photon, respectively. Note that the pump has extraordinary polarization. For an extraordinary ray that is not traveling in the optical axis (OA) direction, the effective refractive index is given by

$$n_{\text{eff}}(\lambda_e, \varphi_e) = \sqrt{\frac{\cos^2(\varphi_e)}{n_o^2(\lambda_e)} + \frac{\sin^2(\varphi_e)}{n_e^2(\lambda_e)}} \tag{2.20}$$

where $_e$ is the wavelength of the extraordinary field, φ_e is the angle between the extraordinary photon and the optical axis inside the crystal, $_e$ is the extraordinary refractive index and $_o$ is the ordinary refractive index. The wavevector for extraordinary and ordinary waves is then

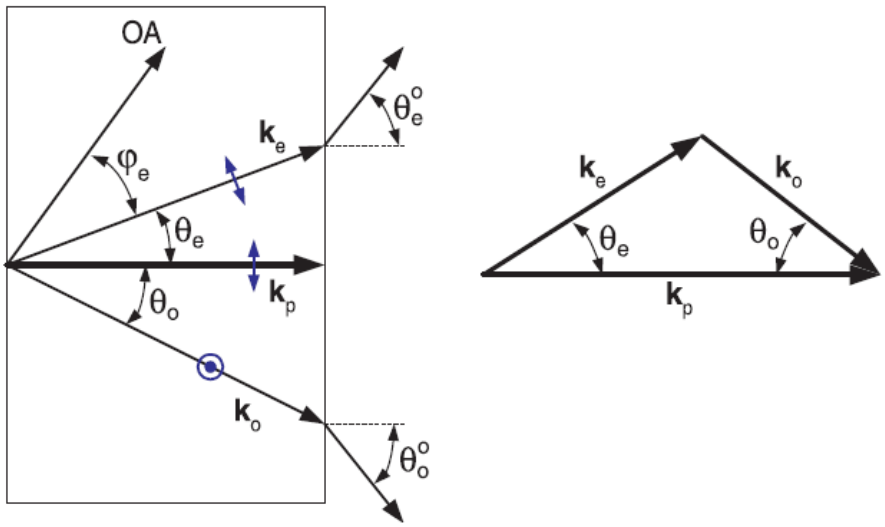

Figure 2.1: non-collinear type-II phase matching in the planar case. Note that all wavevectors lie in the plane defined by the OA and the pump wavevector (k_p), the angle between OA and k_p is $\Psi = \theta_e + \varphi_e$. k_p and k_e are polarized in the direction of extraordinary ray ($\updownarrow$) and k_o is polarized in the direction of ordinary ray ($\odot$). Adapted from Ref. [45].

$$\begin{aligned} k_p(\lambda_p, \Psi) &= \frac{2\pi n_{\text{eff}}(\lambda_p, \Psi)}{\lambda_p}, \\ k_e(\lambda_e, \Psi) &= \frac{2\pi n_{\text{eff}}(\lambda_e, \varphi_e)}{\lambda_e}, \\ k_o(\lambda_o) &= \frac{2\pi n_o(\lambda_o)}{\lambda_o} \end{aligned} \tag{2.21}$$

where Φ is the angle between the pump wave and the optical axis, solving Eq. (2.19) for k_o,

$$k_o(\lambda_o)\cos\theta_o = \sqrt{k_o^2(\lambda_o) - k_e^2(\lambda_e, \varphi_e)\sin^2\theta_e} \tag{2.22}$$

then we replace these results with the Eq. (2.22) on the Eq. (2.19)

$$k_e\cos\theta_e + \sqrt{\left[\frac{2\pi n_o(\lambda_o)}{\lambda_o}\right]^2 - \left[\frac{2\pi n_{\text{eff}}(\lambda_e, \varphi_e)}{\lambda_e}\right]^2 \sin^2\theta_e} = \frac{2\pi n_{\text{eff}}(\lambda_p, \Psi)}{\lambda_p} \tag{2.23}$$

Using the energy conservation from Eq. (2.17) and knowing that $\lambda = \frac{2\pi c}{\omega}$, the expression for the energy conservation is the following

$$\lambda_o = \frac{\lambda_e \lambda_o}{\lambda_e - \lambda_p}$$

The internal angle θ_e can then be converted to the outside angle θ_e^o and θ_o^o by using Snell's law, with

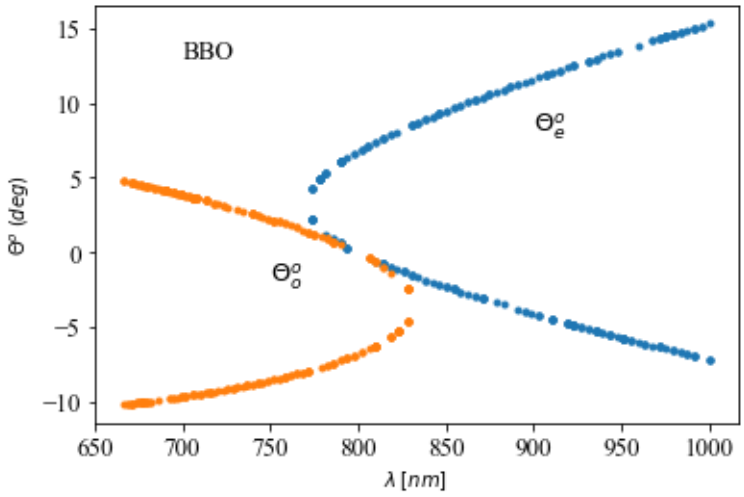

Figure 2.2: Tuning curve for BBO (negative uniaxial) Type II SPDC, with a pump wavelength of 400nm and a θ_c of 42.347deg.

an outside refractive index $n_i = 1$, this means that the photon is coming from the air to the crystal. The e-polarization outside angle is

$$\theta_e^o = \sin^{-1}(n_{\text{eff}}(\lambda_e, \varphi_e)\sin\theta_e) \tag{2.24}$$

and the o-polarization outside angle is

$$\theta_o^o = \sin^{-1}\left(\frac{\lambda_o}{\lambda_e} n_{\text{eff}}(\lambda_e, \varphi_e)\sin\theta_e\right) \tag{2.25}$$

The outside angles θ_e^o, θ_o^o as a function of λ for a fixed λ_p are known as the "tuning curves" for Type-II SPDC. In Fig. 2.2 we show the tuning curves for a BBO crystal with a fixed value of $\lambda_p = 400\text{nm}$ and a $_c = 42.347\text{deg}$.

2.3 Hermite-Gauss Basis

To make the subsequent calculations of the canonical quantization of the electromagnetic field simpler, we express the transverse momentum components of the field in terms of Hermite-Gaussian modes. Let $\mathbf{q}$ denote the projection of the momentum $\mathbf{k}$ onto the transverse plane so that $\mathbf{k} = \mathbf{q} + \mathbf{k}_z\hat{z}$ and $\hat{z}$ is the propagation direction along the optical axis, this means $\Phi = 0$. Since both plane waves and Hermite–Gaussian wavefunctions form a complete basis in 2D space, we can express the creation operator as a sum over the transverse mode creation operator $a^\dagger_{(\vec{\mu},k_z,s)}$, indexed by s (which can take one of two values for each transverse direction), where $\vec{\mu}$ is a vector denoting the horizontal and vertical indices of a Hermite–Gaussian mode of the form (Here, $\vec{\mu}$ is an ordered pair of non-negative integers corresponding to the horizontal and vertical mode index, respectively).

$$a^\dagger_{(\vec{q},k_z,s)} = \sum_{\vec{\mu}} \widetilde{C}_{\vec{q},\vec{\mu}}\; a^\dagger_{(\vec{\mu},k_z,s)} \tag{2.26}$$

this change of basis is unitary. With this established, we can express the displacement field operator $\hat{D}^-(\vec{r},t)$ in terms of the Hermite–Gauss basis.

The transverse spatial dependence $\hat{D}^-(\vec{r},t)$ for a given Hermite–Gauss mode indexed by $\vec{\mu}$ relies on the sum

$$\sum_{\vec{q}} \widetilde{C}_{\vec{\mu},\vec{q}}\, e^{-\vec{q}\cdot\vec{r}} = \sqrt{L_x L_z}\, g_{\vec{\mu}}(x,y) \tag{2.27}$$

where we have defined $g_{\vec{\mu}}(x,y)$ to be the normalized Hermite–Gaussian wavefunction associated with the index $\vec{\mu}$. Finally, using the paraxial approximation (so that the frequency ω only depends on k_z), the displacement field operator becomes

$$\hat{D}^-(\vec{r},t) = -i \sum_{\vec{\mu},k_z,s} \sqrt{\frac{\epsilon_0 n_{k_z}^2 \hbar\omega_{k_z}}{2L_z}}\, \vec{\epsilon}_{k_z,s}\; g_{\vec{\mu}}(x,y) e^{-ik_z z} e^{i\omega t} \hat{a}^\dagger_{\vec{\mu},k_z,s} \tag{2.28}$$

here, we point out that $\hat{a}^\dagger_{\vec{\mu},k_z,s}(t) = e^{i\omega t}\hat{a}^\dagger_{\vec{\mu},k_z,s}$ with this displacement field operator expressed in this new basis (Hermite-Gaussian), we are ready to obtain a nonlinear Hamiltonian, similar to Eq. (2.12).

We consider a monochromatic pump beam with peak magnitude $|D_p^0|$, frequency ω_p, polarization ϵ_p, and (non-normalized) spatial dependence $f_p(\vec{r})$ given by

$$\vec{D}_p(\vec{r},t) = |D_p^0|\vec{\epsilon}_p f_p(\vec{r})\cos(\omega_p t) \tag{2.29}$$

we can factor out the linear phase due to propagating the beam, giving us:

$$f_p(\vec{r}) = \tilde{G}_p(\vec{r})e^{-ik_z z} \tag{2.30}$$

where $\tilde{G}_p(\vec{r})$ will describe the rest of the Gaussian pump beam, so that:

$$\tilde{G}_p(\vec{r}) = \frac{\sigma_p}{\sigma(z)} exp(-\frac{x^2+y^2}{4\sigma(z)^2}) exp(-ik_z \frac{x^2+y^2}{2R(z)}) exp(itan^{-1}(\frac{z}{z_r})) \tag{2.31}$$

The first term of Eq. (2.31) governs the evolving spatial amplitude of the beam; the second exponential describes the propagation and curvature of the phase fronts, while the last exponential describes the Guoy phase. we use the simplifying approximation that the pump beam is collimated, so that we may neglect the Guoy phase and curvature of the phase fronts in our calculations. $\sigma(z)$ is the evolving beam radius

$$\sigma(z) \equiv \sigma_p \sqrt{1 + (\frac{z}{z_r})^2}, \tag{2.32}$$

$R(z)$ is the evolving radius of curvature of the wavefronts

$$R(z) \equiv z\left[1 + \left(\frac{z}{z_r}\right)^2\right], \qquad z_R \equiv \frac{4\pi\sigma_p^2}{\lambda_p} \tag{2.33}$$

and z_r is the Rayleigh length, such as $\sigma(z_r) = \sqrt{2}\sigma_p$.

The power delivered by the Gaussian pump beam, in units of energy per second is then

$$P = c\frac{|D_p^0|^2}{n^3\epsilon_0}\pi\sigma_p^2 \tag{2.34}$$

which is equal to the mean intensity of the beam times its effective area.

Including these expressions for the displacement field operators and the classically bright pump field, the nonlinear effective Hamiltonian that describes SPDC becomes

$$\begin{aligned} \hat{H}_{NL} \quad = \quad & \int d^3r(\zeta_{eff}^{(2)}|D_p^0|\tilde{G}_p^* e^{ik_{pz}z}e^{i\omega pt} \\ & \times -i\sum_{\mu_1,k_{1z}} \sqrt{\frac{\epsilon_0 n_1^2\hbar\omega_1}{2L_z}} g_{\mu_1}(x,y)e^{-ik_{1z}z}e^{i\omega_1 t}\hat{a}^\dagger_{\vec{\mu_1},k_{1z},s} \\ & \times -i\sum_{\mu_2,k_{2z}} \sqrt{\frac{\epsilon_0 n_2^2\hbar\omega_2}{2L_z}} g_{\mu_2}(x,y)e^{-ik_{2z}z}e^{i\omega_2 t}\hat{a}^\dagger_{\vec{\mu_2},k_{2z},s} + H.c.) \end{aligned} \tag{2.35}$$

where $\zeta^{(2)}_{eff}$ is the effective second-order inverse optical susceptibility tensor. Furthermore, we have already performed the sum over the components of the inverse susceptibility. After algebraic simplifications, we obtain

$$\begin{aligned}\hat{H}_{NL} &= \frac{\hbar|E_p^0|}{2L_z}\sum_{\mu_1,k_{1z}}\sum_{\mu_2,k_{2z}}\sqrt{\frac{\omega_1\omega_2}{n_1^2 n_2^2}}\int d^3r(\chi^{(2)}_{eff}(\vec{r})G^*_p(\vec{r})g_{\vec{\mu}_1}(x,y)g_{\vec{\mu}_2}(x,y)e^{-i\Delta k_z z}) \\ &\times e^{i\Delta\omega t}\hat{a}^\dagger_{\vec{\mu_1},k_{1z},s}\hat{a}^\dagger_{\vec{\mu_2},k_{2z},s} + H.c. \end{aligned} \tag{2.36}$$

here we have switched from $\zeta^{(2)}_{eff}$ to the effective nonlinear susceptibility $\chi^{(2)}_{eff}$ using the following approximation:

$$-\epsilon_0^2\,\zeta^2_{eff}\,n_p^2\,n_1^2\,n_2^2 \approx \chi^{(2)}_{eff} \tag{2.37}$$

which is satisfied under the same lossless media assumption that allowed us to invoke full permutation symmetry [46].

2.4 Effective Nonlinearity

Considering the polarization inside a nonlinear material as:

$$P_i(t) = \epsilon_0 \chi_{ij}^{(1)} E_j(t) + \epsilon_0 \chi_{ijk}^{(2)} E_j(t) E_k(t) + ... \tag{2.38}$$

where $\chi_{ij}^{(1)}$ and $\chi_{ijk}^{(2)}$ are the first-order linear susceptibility tensor and the second-order nonlinear susceptibility tensor, respectively.

The electric displacement vector is given by

$$D(r,\omega) = \epsilon_0 E(r,\omega) + P(r,\omega) \tag{2.39}$$

The polarization vector can be written as the sum of the linear part and a nonlinear part

$$P(r,\omega) = P^L(r,\omega) + P^{NL}(r,\omega) \tag{2.40}$$

The linear part, or the first element in the Eq. (2.1), can be written as

$$P_i^L(r,\omega) = \sum_{j=1}^{3} \epsilon_0 \chi_{ij}^{(1)}(\omega) E_j(r,\omega) \tag{2.41}$$

where $i = 1,2,3$ and $j = 1,2,3$ represent the three cartesian indices x, y, z, respectively. Assuming that the material is homogeneous, we have that $\chi = \chi(\omega)$.

From this, we can rewrite the electric displacement field as

$$D(r,\omega) = \bar{\epsilon}_0 \cdot E(r,\omega) + P^{NL}(r,\omega) \tag{2.42}$$

where $\bar{\epsilon}_0 = \epsilon_0[1 + \chi^{(1)}(\omega)]$, and is called the dielectric tensor. If we only consider the second order of the nonlinear polarization or the second term in Eq. (2.1), the nonlinear polarization can be written as

$$\begin{aligned} P^{NL}(r,\omega) &= P_j^{(2)}(r,\omega) \\ &= \epsilon_0 \int d\omega_a \int d\omega_b \sum_{lm} \chi_{jlm}^{(2)}(\omega_p, \omega_a, \omega_b) \delta(\omega_p - \omega_a - \omega_b) E_l(r,\omega_a) E_m(r,\omega_b) \end{aligned} \tag{2.43}$$

where for SPDC E_l and E_m correspond to the signal and idler electric fields, ω_a, and ω_b are the frequencies for the signal and idler photons.

Since the reality condition also applies to the second-order nonlinear polarization, $\chi_{jml}^{(2)*}(\omega_p, \omega_a, \omega_b) = \chi_{jml}^{(2)}(-\omega_p, -\omega_a, -\omega_b)$. We can start the calculation of the effective nonlinear susceptibility using the

second-order nonlinear susceptibility tensor as [45]

$$d_{ijk} = \frac{\epsilon_0}{2}\chi^{(2)}_{ijk} \tag{2.44}$$

where the effective nonlinearity is given by

$$d_{\text{eff}} = \sum_{ijk} d_{ijk} e^s_i e^i_j e^p_k \tag{2.45}$$

where s, i, p correspond to the signal, idler, and pump beam, respectively, and e_i, e_j, e_k correspond to the polarization vector in the x, y, z cartesian coordinate, respectively. Now we can assume the following conditions, to introduce a symmetry condition of the tensor d_{ijk}. The material is lossless, this implies that we have a full permutation symmetry i.e the indices can be permuted as long as the frequencies are permuted as well.

This condition is called the Kleinman symmetry condition, which implies that the value of d_{eff} is independent of the position of the signal and idler fields in Eq. (2.45).

The d_{ijk} tensor has 27 elements. where i, j, k denote cartesian coordinates. Explicitly we have

$$d_{ijk} = \begin{pmatrix} d_{111} & d_{112} & d_{113} & d_{121} & d_{122} & d_{123} & d_{131} & d_{132} & d_{133} \\ d_{211} & d_{212} & d_{213} & d_{221} & d_{222} & d_{223} & d_{231} & d_{232} & d_{233} \\ d_{311} & d_{312} & d_{313} & d_{321} & d_{322} & d_{323} & d_{331} & d_{332} & d_{333} \end{pmatrix} \tag{2.46}$$

where 1 refers to the x coordinate of the crystal, 2 to the y coordinate, and 3 to the z coordinate. The z coordinate coincides with the optical axis in uniaxial crystals.

For SPDC type II the interaction of polarizations occurs as follows. For negative uniaxial crystals, we have an incident extraordinary polarization and the two orthogonal polarizations as output ($e \Rightarrow e, o$), and for positive uniaxial crystals, we have an incident ordinary polarization and the same output as the negative uniaxial ($o \Rightarrow e, o$). This reduces the number of elements of the tensor that is relevant in Eq. (2.46). For the coordinate system represented in Fig. 2.3 (a) and (b), we can write the components of the electric field of the ordinary ray as

$$\vec{E}_o = E_e o_j \tag{2.47}$$

where,

$$\begin{pmatrix} \sin(\phi) \\ -\cos(\phi) \\ 0 \end{pmatrix} = o_j \tag{2.48}$$

and the components of the extraordinary ray as

$$\vec{E}_e = E_e e_j \tag{2.49}$$

where

$$\begin{pmatrix} -\cos(\theta)\cos(\phi) \\ -\cos(\theta)\sin(\phi) \\ sin(\theta) \end{pmatrix} = e_j \tag{2.50}$$

where ϕ is the projection of the propagation vector in the plane $y_c - x_c$ of Fig. 2.3 (a), and for collinear SPDC θ is equaled to θ_c is the angle between the normal to the incident plane and the OA.

For type II SPDC in a negative uniaxial crystal the polarization is calculated as

$$P^e_{eo}(\omega_3) = e_i d_{ijk}(\omega_3, \omega_2, \omega_1) e_j o_k E_j(\omega_2) E_k(\omega_1) \tag{2.51}$$

and for a positive uniaxial crystal, we have that

$$P^o_{eo}(\omega_3) = o_i d_{ijk}(\omega_3, \omega_2, \omega_1) e_j o_k E_j(\omega_2) E_k(\omega_1) \tag{2.52}$$

where $P(\omega)$ is the dielectric polarization of the crystal at the pump frequency of ω_3. Using the Kleinman symmetry conditions for the Eq. (2.51) and Eq. (2.52) we can swap the position of the extraordinary and ordinary ray of outputs as needed.

For negative uniaxial crystal, we used the expression of Eq. (2.49) and Eq. (2.47) to replace Eq.

(2.51) to obtain

$$
\begin{aligned}
d_{\text{eff}} &= d_{xxx}\cos^2(\theta)\cos^2(\phi)\sin(\phi) - d_{xxy}\cos^2(\theta)\cos^3(\phi) \\
&+ d_{xyx}\cos^2(\theta)\cos(\phi)\sin^2(\phi) - d_{xyy}\cos^2(\theta)\cos^2(\phi)\sin(\phi) \\
&- d_{xzx}\cos(\theta)\sin(\theta)\cos(\phi)\sin(\phi) + d_{xzy}\cos(\theta)\sin(\theta)\cos^2(\phi) \\
&+ d_{yxx}\cos^2(\theta)\sin^2(\phi)\cos(\phi) - d_{yxy}\cos^2(\theta)\cos^2(\phi)\sin(\phi) \\
&+ d_{yyx}\cos^2(\theta)\sin^3(\phi) - d_{yyy}\cos^2(\theta)\sin^2(\theta)\cos(\theta) - d_{yzx}\cos(\theta)\sin(\theta)\sin^2(\phi) \\
&+ d_{yzy}\cos(\theta)\sin(\theta)\cos(\phi)\sin(\phi) - d_{zxx}\sin(\theta)\cos(\theta)\cos(\phi)\sin(\phi) \\
&+ d_{zxy}\sin(\theta)\cos(\theta)\cos^2(\phi) - d_{zyx}\sin(\theta)\cos(\theta)\sin^2(\phi) \\
&+ d_{zyy}\sin(\theta)\cos(\theta)\sin(\phi)cos(\phi) + d_{zzx}\sin^2(\theta)\sin(\phi) - d_{zzy}\sin^2(\theta)\cos(\phi)
\end{aligned}
\tag{2.53}
$$

analogously we can obtain a similar expression but for positive uniaxial using the Eq. (2.52).

2.5 Glauber two-photon correlation function

The spectral and temporal properties of the biphoton state, as the state in Eq. (1.2), is determined by the joint spectral function ($\Phi(\Delta k)$), Eq. (2.16). The arrival times for all the photon pairs emitted by the crystal are detected in a coincidence setup and the probability of detecting two-photon pairs at diferent times t_1 and t_2 are proportional to the correlation function $G^{(2)}(t_1, t_2)$ is given by

$$
G^{(2)}(t_1, t_2) = |\langle 0| \left(\hat{E}^{(+)}(t_2)\hat{E}^{(+)}(t_1)\right) |\Psi_2\rangle|^2 \tag{2.54}
$$

where the electric field operators are given by Eq. (2.6) and take into account any spectral filtering done at the detectors. If we assume that this correlation depends only on a relative time $\tau = t_1 - t_2$, this can be done because we are only considering the pump as a Gaussian beam and the Hermite-Gauss basis for the two generated photons, in other words, there is not a spatial dependency for the correlation assuming a Hermite-Gauss basis for the generated photons. The right-hand side of Eq. (2.54) is proportional to the frequency spectrum of the light as

$$
G^{(2)}(\tau) \approx |I_0(\tau)|^2 \tag{2.55}
$$

and the frequency spectrum of the light is given by:

$$
I_0(\tau) = \int_{-\infty}^{\infty} d\nu \Phi\left(\frac{\Delta k L}{2}\right) e^{-\left(\frac{v^2}{\sigma^2}\right)} e^{-i\nu\tau} \tag{2.56}
$$

where ν is a small detuning frequency and $\Phi(x)$ is known as the joint spectral function (JSA) of the Eq. (2.16) [45].

Now for type II SPDC the expansion of k with respect to detuning from perfect phase matching can be expressed

$$k_i = K_i + v\frac{dk_i}{d\omega_i}\bigg|_{\Omega_i} \tag{2.57}$$

where the expansion was made around the central frequency of the Gaussian beam ω_i and K_i is the wavevector with a frequency of ω_i, $\Omega_i = \omega_i \pm \nu$, and $i = o, e$ correspond to the ordinary and the extraordinary rays respectively. Since $\Delta k = 0$ at perfect phase matching, we have

$$\Delta k = \nu D \tag{2.58}$$

where

$$D = \frac{dk_o}{d\omega_o}\bigg|_{\Omega_o} - \frac{dk_e}{d\omega_e}\bigg|_{\Omega_e} \tag{2.59}$$

Ω_o and Ω_e as the central frequencies for the ordinary and the extraordinary waves respectively, the two derivatives expressions in Eq. (2.59) are the inverse of the group velocity and can be derived numerically from the Sellmeier equation of the crystal. The Glauber correlation function for Type II SPDC is then given by

$$G^{(2)}(\tau) \approx \left| \int_{-\infty}^{\infty} d\nu \Phi(vDL/2) e^{-\left(\frac{\nu^2}{\sigma^2}\right)} e^{-iv\tau} \right|^2 \tag{2.60}$$

where $\Phi(x)$ is the JSA of the Eq. (2.16), but because we neglected the amplitudes the joint spectral function is proportional to the $\mathrm{sinc}(\nu DL/2)$, and σ corresponds to the bandwidth of the filter in the detector and $\tau = t_1 - t_2$ with t_1 and t_2 are the detection times for the two generated photons. In Fig. 2.4, we show the Glauber biphoton correlation function for a BBO crystal with a pump wavelength of $532\mathrm{nm}$ and a detector bandwidth of $1\mathrm{nm}$.

From the Glauber correlation function, we can obtain a correlation time between the two photons generated by the SPDC. For BBO (Fig. 2.4) this correlation time is $441.806\mathrm{fs}$.

2.6 Biphoton generation rate

Using first-order time-dependent perturbation theory, we can calculate the biphoton rate. To do so, we take the initial state of the down-converted fields to the vacuum state and the final state to be a biphoton with a Hermite-Gauss mode number and momenta (k_{nz}, $\vec{\mu}_n$) with $n = 1, 2$ representing the signal and idler photon. The transition probability is given by:

$$\begin{aligned} P_{k_{1z},\vec{\mu}_1,k_{2z},\vec{\mu}_2} &\equiv |\langle \vec{\mu}_1, k_{1z}, \vec{\mu}_2, k_{2z}|\Psi(t)\rangle|^2 \\ &\approx |\langle \vec{\mu}_1, k_{1z}, \vec{\mu}_2, k_{2z}| \left(1 - \frac{i}{\hbar}\int_0^t dt' H_{NL}(t')\right)|0,0\rangle|^2 \end{aligned} \tag{2.61}$$

Where the expression in parenthesis comes from the first-order perturbation theory of the time propagation operator. Substituting the non-linear Hamiltonian expression on the Eq. (2.61), we obtain

$$\begin{aligned} P_{k_{1z},\vec{\mu}_1,k_{2z},\vec{\mu}_2} &= \frac{|E_p^0|^2}{4L_z^2}\frac{\omega_1\omega_2}{n_1^2 n_2^2} \\ &\times \left|\int d^3r(\chi^2_{eff}(\vec{r})G_p^*(\vec{r})g_{\vec{\mu}_1}(x,y)g_{\vec{\mu}_2}(x,y)e^{-i\Delta k_z z})\right|^2 \left|\int_0^t e^{i\Delta\omega t'}\right|^2 \end{aligned} \tag{2.62}$$

where we can define

$$\begin{aligned} W_{k_{1z},\vec{\mu}_1,k_{2z},\vec{\mu}_2} &= \frac{|E_p^0|^2}{4L_z^2}\frac{\omega_1\omega_2}{n_1^2 n_2^2} \\ &\times \left|\int d^3r(\chi^2_{eff}(\vec{r})G_p^*(\vec{r})g_{\vec{\mu}_1}(x,y)g_{\vec{\mu}_2}(x,y)e^{-i\Delta k_z z})\right|^2 \end{aligned} \tag{2.63}$$

to simplify the notation. We can further simplify this expression by using the fact that the magnitude of a complex number does not depend on the phase

$$\begin{aligned} P_{k_{1z},\vec{\mu}_1,k_{2z},\vec{\mu}_2} &= W_{k_{1z},\vec{\mu}_1,k_{2z},\vec{\mu}_2}\left|\mathrm{sinc}\left(\frac{\Delta\omega t}{2}\right)t\right|^2 \\ &\times \left|\int_0^t dt' e^{i\Delta\omega t'}\right|^2 \end{aligned} \tag{2.64}$$

and taking into consideration that we can take the limit when t becomes large, we obtain

$$P_{k_{1z},\vec{\mu}_1,k_{2z},\vec{\mu}_2} \approx W_{k_{1z},\vec{\mu}_1,k_{2z},\vec{\mu}_2}(2\pi\delta(\Delta\omega))\left|\int_0^t dt' e^{i\Delta\omega t'}\right| \tag{2.65}$$

In practice, we need t to be much larger than the inverse of $\Delta\omega$, this can be archived for times much longer than picosecond times scales that light takes to travel through the crystal, but not so large that multiple biphotons are likely to be generated in time t. The range of frequencies defining the width $\Delta\omega$

is known as the phase matching bandwidth, and commonly is in the range of $10^{-13} - 10^{-14}$ seconds for known optical crystals. Now we can define the transition rate as $R_{k_{1z},\vec{\mu}_1,k_{2z},\vec{\mu}_2}$ is defined as the time derivative of the transition probability P, and if we take times much longer than picosecond this transition rate is constant and have the following form:

$$R_{k_{1z},\vec{\mu}_1,k_{2z},\vec{\mu}_2} \approx W_{k_{1z},\vec{\mu}_1,k_{2z},\vec{\mu}_2} 2\pi\delta(\Delta\omega) \tag{2.66}$$

To calculate the total transition rate for down conversion into a single pair of transverse modes $R_{\vec{\mu}_1,\vec{\mu}_2}$, we must add all the transition rates for all values of k_{1z} and k_{2z}:

$$R_{\vec{\mu}_1,\vec{\mu}_2} = \sum_{k_{1z},k_{2z}} R_{k_{1z},\vec{\mu}_1,k_{2z},\vec{\mu}_2} \tag{2.67}$$

if we take in consideration that the large of the crystal L_z is much longer than the wavelength of the light passing through it, we can approximate the sums over k_{1z} and k_{2z} as integrals:

$$\sum \approx \left(\frac{L_z}{2\pi}\right)^2 \int dk_{1z} dk_{2z} \tag{2.68}$$

now this equation can be expressed as an integral over the frequencies as the following expression:

$$\left(\frac{L_z}{2\pi}\right)^2 \int dk_{1z} dk_{2z} \approx \left(\frac{L_z}{2\pi}\right)^2 \frac{n_{g1} n_{g2}}{c^2} \int d\omega_1 d\omega_2, \tag{2.69}$$

where n_{g1} and n_{g2} are the group index at the signal and idler frequency respectively. The single-mode transition rate $R_{\vec{\mu}_1,\vec{\mu}_2}$ is thus given by

$$R_{\vec{\mu}_1,\vec{\mu}_2} = \int d\omega_1 d\omega_2 W_{k_{1z},\vec{\mu}_1,k_{2z},\vec{\mu}_2} \frac{L_z^2 n_{g1} n_{g2}}{2\pi c^2} \delta(\Delta\omega), \tag{2.70}$$

where $W_{k_{1z},\vec{\mu}_1,k_{2z},\vec{\mu}_2}$ is expressed in terms of the frequencies ω_1 and ω_2. Then the total rate R is the sum over all transverse modes $\vec{\mu}_1$ and $\vec{\mu}_2$of the single-mode rates.

2.7 The bulk crystal regime: photon-pair brightness

The biphoton generation rate depends on the overlap integral $\Phi(\Delta k_z)$, this function is called the joint spectral function Eq. (2.16)

$$|\Phi(\Delta k_z)|^2 \equiv \left| \int d^3r \left(\chi^2_{eff}(\vec{r}) G^*_p(\vec{r}) g_{\vec{\mu}_1}(x,y) g_{\vec{\mu}_2}(x,y) e^{-i\Delta k_z z} \right) \right|^2 \tag{2.71}$$

The simplest case to solve is that of the collimated Gaussian pump beam incident on an isotropic rectangular crystal of dimensions $L_x \times L_y \times L_z$ centered at the origin of a Cartesian coordinate system with $\hat{z}$ pointing along the optic axis. If we make the additional assumption that we are collecting the down-converted light into single-mode fibers, then only the photons generated in the zeroth-order Hermite–Gaussian modes will contribute to the rate of detected events. In this case, $G_p(\vec{r})$, $g_{\vec{\mu}_1}$, and $g_{\vec{\mu}_2}$ are all Gaussian functions, so that $|\Phi(\Delta k_z)|^2$ becomes

$$\begin{aligned} |\Phi(\Delta k_z)|^2 \quad = \quad & \left(\frac{\chi^{(2)}_{eff}}{2\pi\sigma_1^2} \right)^2 \left| \int_{L_z/2}^{-L_z/2} dz e^{-i\Delta k_z z} \right|^2 \\ & \times \left| \int dx dy \quad e^{\left[-(x^2+y^2)\left(\frac{1}{4\sigma_p^2} + \frac{2}{4\sigma_1^2} \right) \right]} \right| \end{aligned} \tag{2.72}$$

where we assume that the filters for both detectors have the same bandwidth $\sigma_1 = \sigma_2$. To make the limits of the integral over x and y arbitrarily large, it only suffices that the transverse width of the crystal is larger than the dimensions of both the Gaussian pump beam and of the signal and idler modes. Moreover, in single-mode nonlinear waveguides, light can be confined to a much smaller beam diameter without diverging. With these assumptions, the overlap integral simplifies significantly to

$$|\Phi(\Delta k_z)|^2 = (2\chi^2_{\text{eff}} L_z)^2 \text{sinc}^2 \left(\frac{\Delta k_z L_z}{2} \right) \left| \frac{\sigma_p^2}{\sigma_1^2 + 2\sigma_p^2} \right|^2 \tag{2.73}$$

Now we can have an expression for the total rate for down-conversion, R, using as a Gaussian beam the pump beam into another Gaussian signal-idler mode, in terms of the signal and idler frequencies ω_1 and ω_2 as

$$R = \int d\omega_1 d\omega_2 \frac{|E_p^0|^2 (\chi^{(2)}_{eff})^2 L_z^2}{2\pi c^2} \frac{n_{g1} n_{g2}}{n_1 n_2} \left| \frac{\sigma_p^2}{\sigma_1^2 + 2\sigma_p^2} \right|^2 \omega_1 \omega_2 \delta(\Delta\omega) \text{sinc}^2 \left(\frac{\Delta k_z L z}{2} \right) \tag{2.74}$$

where from energy conservation we have that

$$\omega_p = \omega_1 + \omega_2 \tag{2.75}$$

Now we can integrate over one of the frequencies using the delta function in this case, we gonna integrate over the frequency ω_2 to obtain

$$R = \int d\omega_1 \frac{|E_p^0|^2(\chi_{\text{eff}}^{(2)})^2 L_z^2}{2\pi c^2} \frac{n_{g1} n_{g2}}{n_1 n_2} \left| \frac{\sigma_p^2}{\sigma_1^2 + 2\sigma_p^2} \right|^2 \omega_1(\omega_p - \omega_1)\text{sinc}^2\left(\frac{\Delta k_z L z}{2}\right) \tag{2.76}$$

where the phase matching is

$$\Delta k_z = k(\omega_1) + k(\omega_p - \omega_1) - k(\omega_p) \tag{2.77}$$

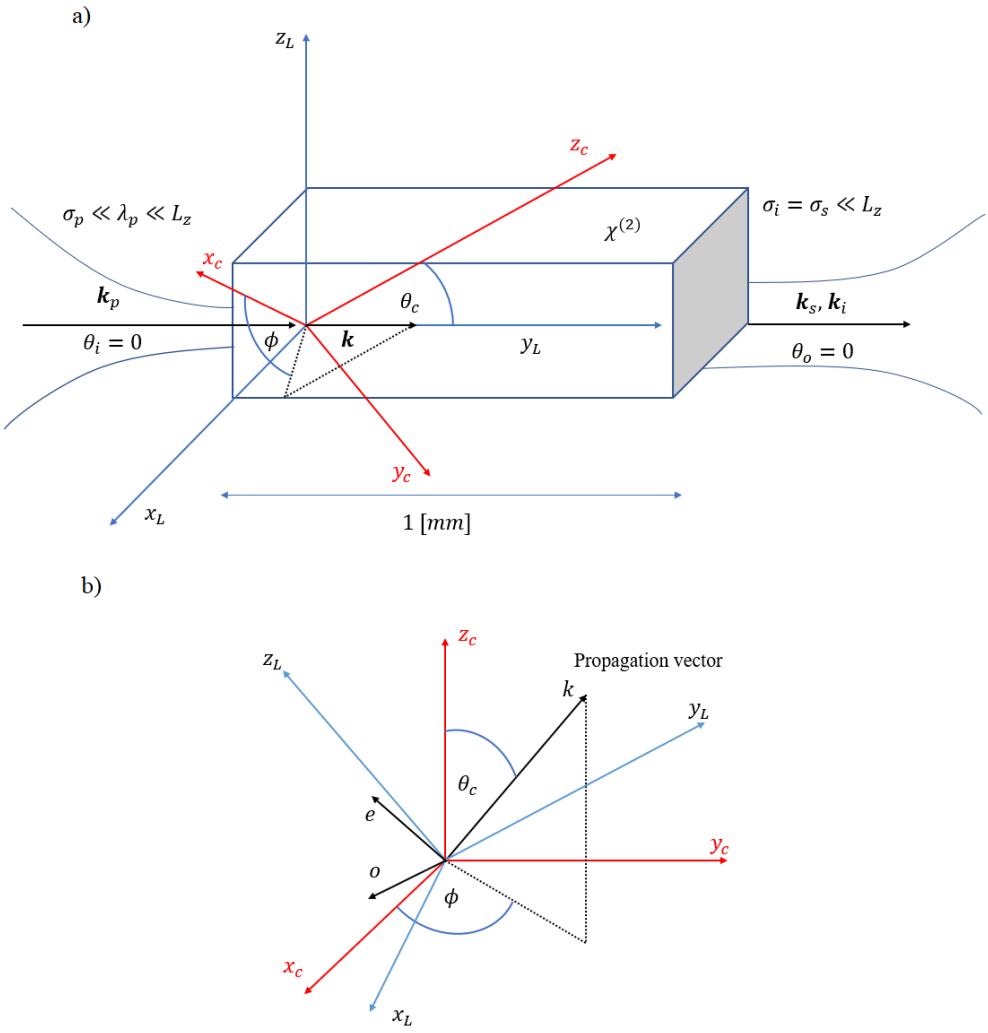

Figure 2.3: Configuration for the estimation of the d_{eff}, where the superscripts L and C correspond to the laboratory frame (blue axis) and crystal frame (red axis) respectively, the o corresponds to the ordinary ray, e corresponds to the extraordinary ray and θ_c is the angle between the optic axis and the propagation vector, for this work this θ_c is equal to the phase matching angle (θ_{PM}) due to the collinear conditions assumed, $\mathbf{k}_p$ is the pump photon, $\mathbf{k}_s$ and $\mathbf{k}_i$ are the signal and idler photons respectively, and $\mathbf{k}$ is the photon inside the crystal, σ_p is the bandwidth of the Gaussian pump beam, and σ_s and σ_i correspond to the bandwidth of the signal and idler photons respectively. Where (a) correspond to the lab frame and (b) the crystal frame.

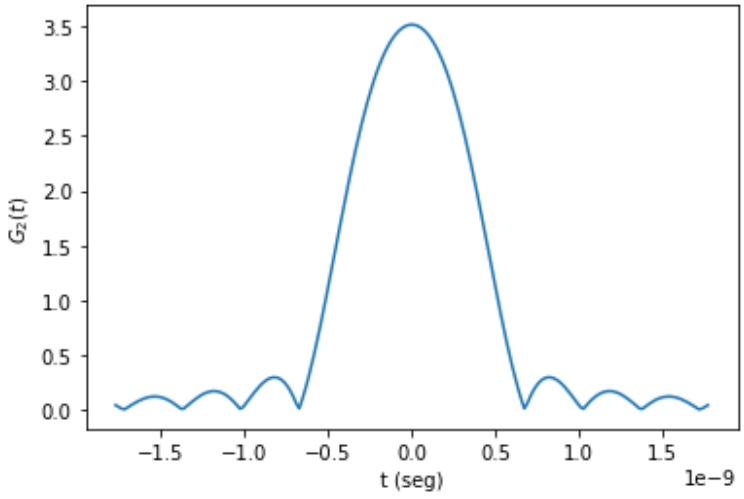

Figure 2.4: $G^{(2)}$ function for BBO with a pump wavelength of $532\mathrm{nm}$ and a θ_c of $42.347\mathrm{deg}$, this function was calculated using Eq. (2.60).

Chapter 3

Type II SPDC in metal-organic frameworks waveguides

For this Thesis, we focus on three MOF crystals: MIRO-101, MIRO-102, and MIRO-103. Previously work was done for Type I degenerate collinear SPDC for the three MOFs of interest by the investigation group [34]. MIRO-101 and MIRO-102 are uniaxial crystals and MIRO-103 corresponds to a biaxial crystal, which as we saw in Chapter 1.2, can always be treated as a uniaxial crystal if we take control of the crystal orientation.

In this chapter, we compute the numerical effectiveness of a crystal to generate entanglement photon pairs by SPDC using the single-mode waveguide counting rate, given by Eq. (2.76).

The calculation of biphoton entangled state in Type II SPDC can be summarized by the following steps:

1. Get Sellmeier equation from the crystal structure via ab initio calculations of electronic structure such as density-functional theory (DFT).

2. Obtain the tuning curves from Eq. (2.25) and Eq. (2.24), using the Sellmeier equations for the crystal. The tuning curves give access to the outside angles, where the photon pair may be detected for a given pump wavelength (λ_s and λ_i). In this thesis, we focus on coplanar degenerate type II SPDC, which means that the target outside angles are zero and $\lambda_s = \lambda_i$.

3. Calculate the group velocity of the two refractive indexes, n_o and n_e, at the signal and idler wavelength using the Sellmeier equation.

4. Calculate the effective nonlinearity of the crystal with the same optical axis that was used for the tuning curves, this d_{eff} can be maximized relative to Φ, using for example the Eq. (2.53), for Type II negative uniaxial.

5. Calculate the $G^{(2)}$ function around the perfect phase matching to estimate a correlation time.

6. Calculate using the correlation time, the d_{eff} optimized, and the group velocity calculated before the numbers of entangled photon pairs generated, via SPDC using Eq. (2.76) to do so.

Following these steps, an estimation of the effectiveness of a crystal to generate entangled biphoton generations can be done and are useful to compare with the crystals typically used in the industry and experiments, such as BBO and KDP.

3.1 Sellmeier equations for MOFs

In this Thesis, all the calculations for Sellmeier equations were previously done using the DFT method in our group [27]. The Sellmeier equations for MIRO-101 are

$$n_o^2 = 2.1078 + \frac{2.51 \times 10^{-2}\lambda^2}{\lambda^2 - 1.41489044 \times 10^5} + \frac{1.0871\lambda^2}{\lambda^2 - 5.62150205 \times 10^4}, \tag{3.1}$$

$$n_e^2 = 1.7833 + \frac{8.9 \times 10^{-3}\lambda^2}{\lambda^2 - 1.44323712 \times 10^5} + \frac{0.36470\lambda^2}{\lambda^2 - 4.9620289 \times 10^4} \tag{3.2}$$

with λ in nm. For MIRO-102 we have

$$n_o^2 = 2.1385 + \frac{1.1527\lambda^2}{\lambda^2 - 4.77658824 \times 10^4} + \frac{7.66 \times 10^{-2}\lambda^2}{\lambda^2 - 1.16666067 \times 10^5}, \tag{3.3}$$

$$n_e^2 = 1.7890 + \frac{5.03 \times 10^{-2}\lambda^2}{\lambda^2 - 1.07012455 \times 10^5} + \frac{0.7432\lambda^2}{\lambda^2 - 3.58417385 \times 10^4} \tag{3.4}$$

and for MIRO-103, we have

$$n_o^2 = 1.9010 + \frac{5.1430 \times 10^{-1}\lambda^2}{\lambda^2 - 5.12308938 \times 10^4} + \frac{0.0408\lambda^2}{\lambda^2 - 1.57385759 \times 10^5}, \tag{3.5}$$

$$n_e^2 = 2.0731 + \frac{1.2882\lambda^2}{\lambda^2 - 5.76235328 \times 10^4} + \frac{0.0107\lambda^2}{\lambda^2 - 1.59071640 \times 10^5} \tag{3.6}$$

Using these Sellmeier equations we calculated the group velocity for k_i and k_s, this group velocities are discussed in Eq. (2.57) as the inverse of $\frac{dk_i}{d\omega_i}$ and $\frac{dk_s}{d\omega_s}$, for signal and idler respectively. The difference between the group velocities of signal and idler is D from Eq. (2.59).

Crystal	$d_{eff}^{(opt)}[\mathrm{pm}V^{-1}]$
MIRO-101	0.72338
MIRO-102	0.16119416
MIRO-103	0.12194346

Table 3.1: d_{eff} optimized for the three MOFs crystals, where 101 and 102 are negative uniaxial and 103 is positive uniaxial.

3.2 Tuning curves

For the calculation of the tuning curves of the MOF crystals, we set the angle between the optical axis (OA) and the normal vector to the plane of incidence, such that $\theta_o^o = 0$ and $\theta_e^o = 0$ for degenerate SPDC type II, as shown in Fig. 2.1. Using the Sellmeier equations from the previous section and Eqs. (2.24,2.25), we can calculate the tuning curves for the MOFs with a pump wavelength $\lambda_p = 532nm$

In Fig. 3.2 (a), (b), and (c) we show the tuning curves for MIRO-101, MIRO-102, and MIRO-103, respectively. Using these tuning curves we obtain the value for the optical axis angle, and as we mention before, to get $\theta_o = \theta_e = 0$ (collinear) for $\lambda_o = \lambda_e$ (non-degenerate) we need to find the appropriate value for the θ_c (optical axis).

3.3 Effective nonlinearlity for MIRO type II phase matching

As we mentioned at the beginning of this Chapter, the effective nonlinearity d_{eff} is calculated using Eq. (2.53) for negative uniaxial crystals, for positive uniaxial we use a similar expression based on Eq.(2.52), we need to use the full tensor d_{ijk} from Eq. (2.46) which was previously calculated by our group [27] for the MOF crystals of interest. In each case (positive or negative uniaxial), the only variable that remains free is the azimuthal angle ϕ, shown in Fig. 3.2, we thus maximize the value of d_{eff} obtaining the curve $d_{\mathrm{eff}}(\Phi)$ and optimizing numerically.

In Fig. 3.3 we show $d_{\mathrm{eff}}(\Phi)$ for the three MOFs of interest. In Table 2.1 we show the optimized values for d_{eff}

3.4 Glauber biphoton correlation function

Assuming a detector bandwidth $\sigma = 1\mathrm{nm}$ and a crystal with thickness $L = 1\mathrm{mm}$, we calculate the Glauber correlation function ($G^{(2)}$) as a function of a time difference $t = t_1 - t_2$, where t_1 and t_2 correspond to the time that a photon is detected on the first detector and the time that a photon is detected on the second detector, respectively. The results are shown in Fig. 3.4 for the three MOFs of interest. Table 3.2 lists the corresponding correlation times for the three MOFs.

From Fig. 3.4, we can obtain the value of the correlation times for all three MOFs, which are in table 3.2.

Crystal	$R \times 10^6[\mathrm{s}^{-1}\mathrm{mW}^{-1}\mathrm{mm}^{-1}]$	$\tau_L[\mathrm{fs}]$
MIRO-101	0.01023349	480.82
MIRO-102	0.0008119	303.68
MIRO-103	0.00040078	566.75

Table 3.2: The number of pair photons generated (R) for second of pumped photons, milliwatts of power pumped and millimeter of the length of the crystal for the three MOFs crystals, and correlation time τ_L by Type II SPDC, where 101 and 102 are negative uniaxial and 103 is positive uniaxial.

3.5 Number of entangled photons pairs generated in collinear SPDC

As we discussed in Section 2.7, we need the value for the bandwidth of the filters for the signal and idler, $\sigma_i = \sigma_s = \sigma_1$, this means that we are using two detectors with the same properties for detecting the signal and the idler photon, and a value for the Gaussian modes for the pump photon σ_p. We use the same values in Ref. [47], for the case of Type II SPDC with a single-mode waveguide of a PPKTP crystal. We thus set $\sigma_1 = 1.875$ and $\sigma_p = 0.875$. The pump wavelength used is the same for the calculation of the tuning curves, $\lambda_p = 532\mathrm{nm}$. The thickness of the crystal is the same used for the calculations of $G^{(2)}$ $L = 1\mathrm{mm}$, this allows to report the number of photon pairs generated by Type II SPDC per second, per milliwatts of pump power, per millimeter. We use Eq. (2.76) to calculate the counting rate of single-mode photon pairs generated R. The value for $d_{\mathrm{eff}}^{(\mathrm{opt})}$ was calculated in the previous section, the Table 3.2 shows the value for the counting rate of biphotons generated by Type SPDC.

We estimate that the most efficient MOF crystal for generating entangled photon pairs via SPDC is MIRO-101. To compare the efficiency of the MIRO-101 to industrial used crystals, we consider the PPKTP crystal [47] with $R = 1.112264 \times 10^6$ per second of pumped photons, milliwatts of power pumped, and millimeters of crystal length. Compared to PPKTP previously mentioned, the MIRO-101 crystal has a 0.92$\%$ of efficiency. Worth mentioning that MOFs are tailor-design crystals, so having a crystal such as the MIRO-101 that has a 1% approximate effectiveness compared to new crystals introduced in the industry, marks a point to study these MOF crystals for designing a new crystal that can be compared with PPKTP or any crystal used in industry.

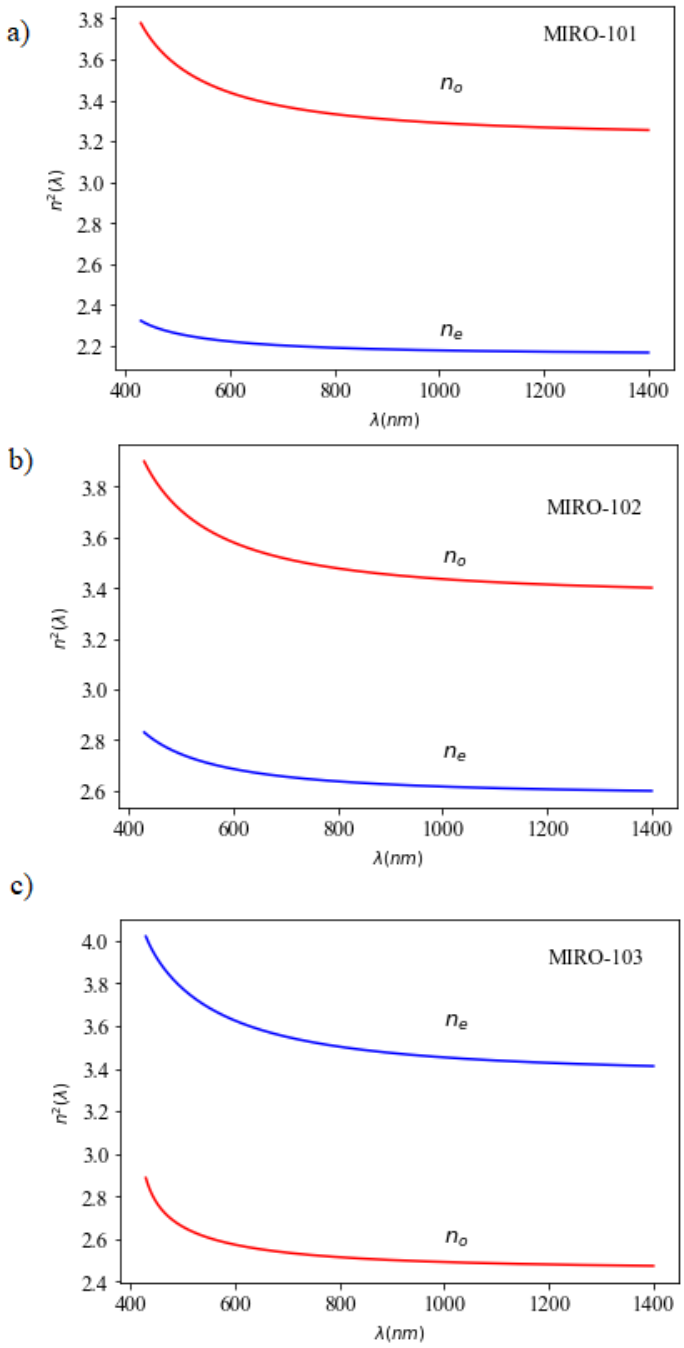

Figure 3.1: Sellmeier equation for (a) MIRO-101 negative uniaxial crystal, (b) MIRO-102 negative uniaxial crystal and (c) MIRO-103 positive uniaxial crystal , where the red line correspond to n_o and the blue line corresponds to n_e from the Eq. (3.1) to Eq. (3.6).

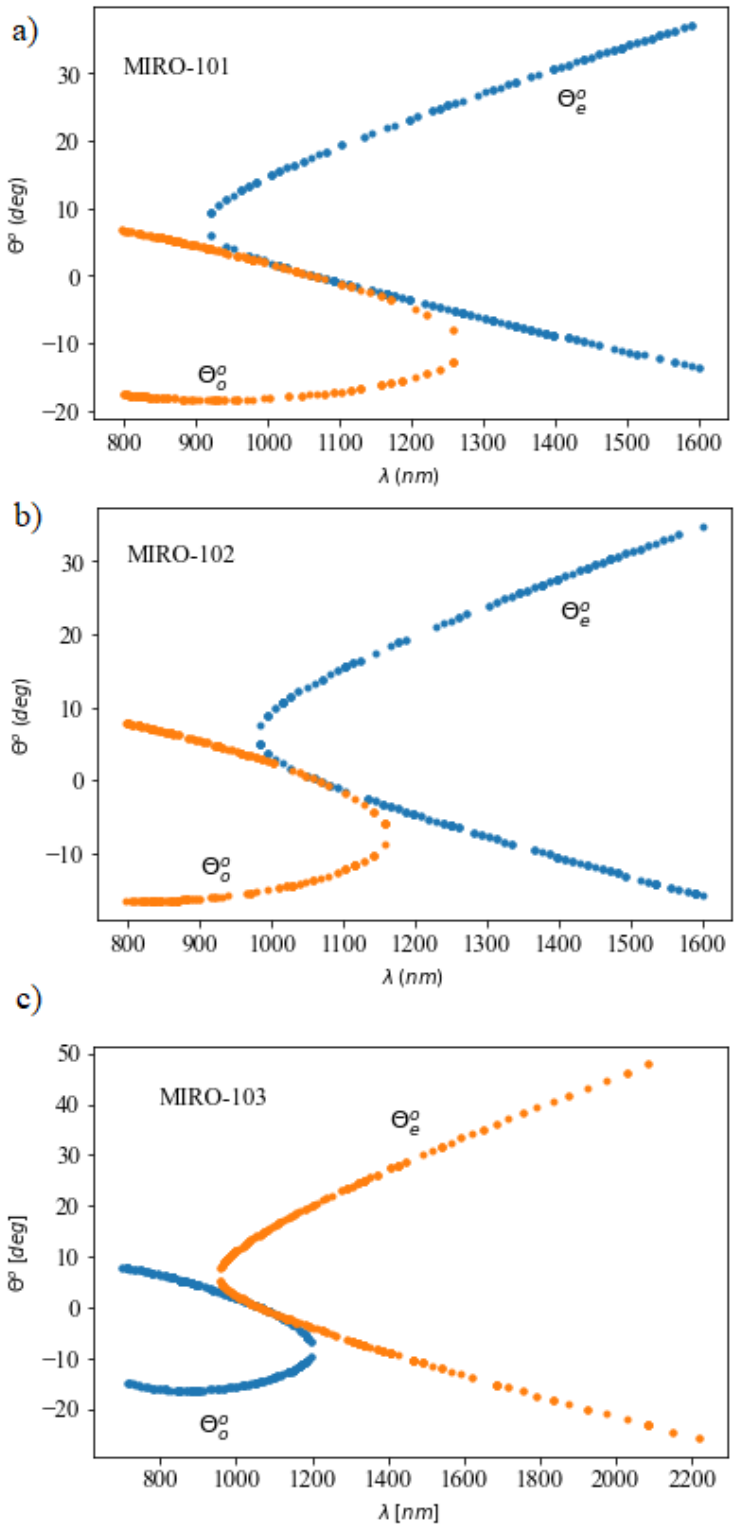

Figure 3.2: Tuning curves for the MOF (a) MIRO-101 (negative uniaxial), $OA = 28.6$, (b) MIRO-102 (negative uniaxial), $OA = 36.85$, (C) MIRO-103 (positive uniaxial), $OA = 36.2$ with a $\lambda_p = 532[nm]$ for the three MOFs, the orange curve correspond to the photon with extraordinary polarization and the blue curve correspond to the photon whit ordinary polarization, and the pump has an ordinary polarization.

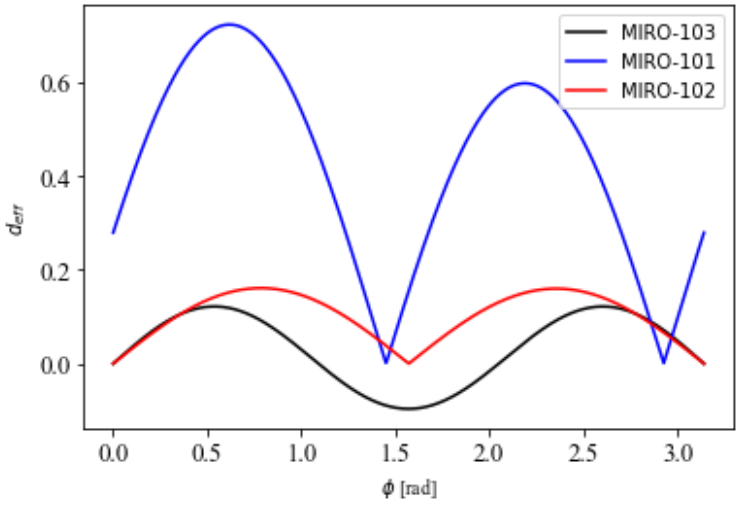

Figure 3.3: Plot of d_{eff} versus the angle of the projection of k in the plane X_c-Y_c (ϕ), from Fig. 3.2, for the three MOF crystals, MIRO-101, MIRO-102 and MIRO-103

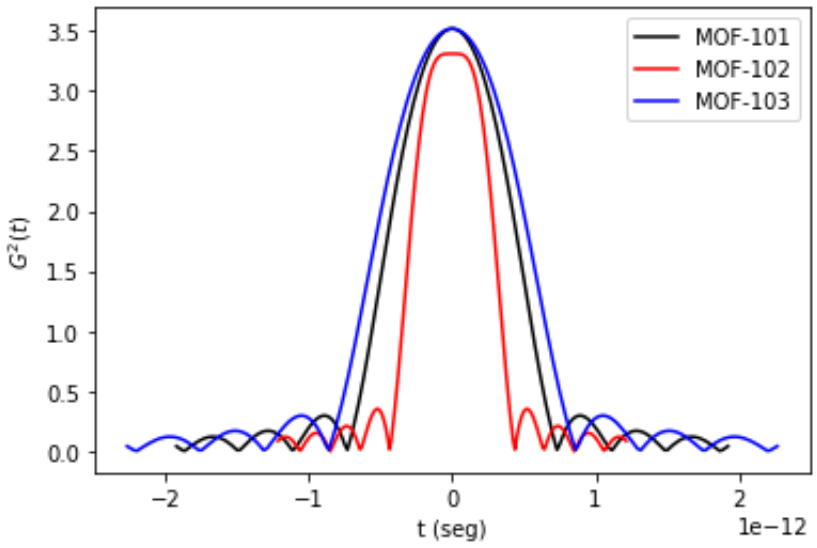

Figure 3.4: Glauber Correlation function (G^2) for the MOFs MIRO 101, MIRO 102, and MIRO 103, where t is the difference time of detection for the two photons generated by SPDC.

Chapter 4

Conclusion and Outlook

In this Thesis, we have calculated the efficiency of nonlinear organic crystals for generating biphoton entangled states. Specifically, we estimated the number of photon pairs generated by spontaneous parametric down-conversion (SPDC) in single-mode waveguides to estimate the efficiency of three Metal-Organic Framework crystal (MOF) MIRO-101, MIRO-102, and MIRO-103 under strong classical pumping. The Theory is summarized at the beginning of Chapter 4. The calculations for the estimation of the nonlinear susceptibility tensor $\chi^{(2)}$ for each MOF were previously done by our group, using density functional theory (DFT). The calculation was done for a pump wavelength of $\lambda_p = 532\mathrm{nm}$ and taking into consideration a Gaussian beam as the pump and for the biphoton generation a Hermite-Gauss basis for the transverse modes waveguide in 2D.

The type of crystals typically used in industry for biphoton entangled generation are BBO, KDP, and Lithium Niobate, in most recent years, quasi-phase matched waveguide crystals are being used to achieve higher SPDC efficiency. For this thesis, we consider new MOF materials as a proof-of-concept to the development of tailor-designed non-linear crystals, which can extend the experimental scope studies of entangled photon pairs generation in quantum technology.

As an outlook, this work can be extended to study large databases of MOF crystals in the literature. In general, we found that MOFs have relative competitive efficiency relative to industrial materials such as quasi-phase matched waveguide crystals. Large-scale studies are feasible because our multi-scale computational method is scalable, which can be useful for studying crystals databases of MOFs and other non-centrosymmetric crystals.

Appendix A

A.1 Phase matching integral

The integral that we need to solve looks like

$$I = \int_{-r/2}^{r/2} e^{-ikx} dx \tag{A.1}$$

solving this integration, we obtain

$$I = \frac{2ie^{(-ikr/2)}}{k} - \frac{2ie^{(ikr/2)}}{k} \tag{A.2}$$

then

$$\frac{2ie^{(-ikr/2)}}{k} - \frac{2ie^{(ikr/2)}}{k} = \frac{2}{k}\left(ie^{(-ikr/2)} - ie^{(ikr/2)}\right) \tag{A.3}$$

where

$$\left(ie^{(-ikr/2)} - ie^{(ikr/2)}\right) = \sin\frac{kr}{2} \tag{A.4}$$

Finally, the integral becomes

$$\frac{2\sin\frac{kr}{2}}{k} = \mathrm{sinc}\frac{kr}{2} \tag{A.5}$$

A.2 SI Units

$\chi^{(2)}$	$[\mathrm{pm}V^{-1}]$
$d_{\mathrm{eff}}^{(2)}$	$[\mathrm{pm}V^{-1}]$
D	$[\frac{\mathrm{m}}{\mathrm{Hz}}]$
λ	$[\mathrm{nm}]$
OA	$[\mathrm{deg}]$

Table A.1: Relevant Units

Bibliography

[1] AV Sergienko, YH Shih, and MH Rubin. “Experimental evaluation of a two-photon wave packet in type-II parametric downconversion”. In: *JOSA B* 12.5 (1995), pp. 859–862.

[2] AV Sergienko et al. “Quantum cryptography using femtosecond-pulsed parametric down-conversion”. In: *Physical Review A* 60.4 (1999), R2622.

[3] Jianwei Wang et al. “Integrated photonic quantum technologies”. In: *Nature Photonics* 14.5 (2020), pp. 273–284.

[4] Thomas Jennewein et al. “Quantum cryptography with entangled photons”. In: *Physical review letters* 84.20 (2000), p. 4729.

[5] Robert W Boyd. *Nonlinear optics*. Academic press, 2020.

[6] Barbara M Terhal. “Detecting quantum entanglement”. In: *Theoretical Computer Science* 287.1 (2002), pp. 313–335.

[7] John S Bell. “On the einstein podolsky rosen paradox”. In: *Physics Physique Fizika* 1.3 (1964), p. 195.

[8] Morton H Rubin et al. “Theory of two-photon entanglement in type-II optical parametric down-conversion”. In: *Physical Review A* 50.6 (1994), p. 5122.

[9] Paul G Kwiat et al. “Proposal for a loophole-free Bell inequality experiment”. In: *Physical Review A* 49.5 (1994), p. 3209.

[10] SP Walborn, S Pádua, and CH Monken. “Hyperentanglement-assisted Bell-state analysis”. In: *Physical Review A* 68.4 (2003), p. 042313.

[11] Michael A Nielsen and Isaac Chuang. *Quantum computation and quantum information*. 2002.

[12] Helle Bechmann-Pasquinucci and Wolfgang Tittel. “Quantum cryptography using larger alphabets”. In: *Physical Review A* 61.6 (2000), p. 062308.

[13] Mohamed Bourennane, Anders Karlsson, and Gunnar Björk. “Quantum key distribution using multilevel encoding”. In: *Physical Review A* 64.1 (2001), p. 012306.

[14] Nicolas J Cerf et al. “Security of quantum key distribution using d-level systems”. In: *Physical review letters* 88.12 (2002), p. 127902.

[15] Paul-Antoine Moreau et al. “Ghost imaging using optical correlations”. In: *Laser & Photonics Reviews* 12.1 (2018), p. 1700143.

[16] Jeffrey H Shapiro. “Computational ghost imaging”. In: *Physical Review A* 78.6 (2008), p. 061802.

[17] Jeffrey H Shapiro and Robert W Boyd. “The physics of ghost imaging”. In: *Quantum Information Processing* 11.4 (2012), pp. 949–993.

[18] Miles J Padgett and Robert W Boyd. “An introduction to ghost imaging: quantum and classical”. In: *Philosophical Transactions of the Royal Society A: Mathematical, Physical and Engineering Sciences* 375.2099 (2017), p. 20160233.

[19] Piotr Ryczkowski et al. “Ghost imaging in the time domain”. In: *Nature Photonics* 10.3 (2016), pp. 167–170.

[20] Lev Vaidman. “Teleportation of quantum states”. In: *Physical Review A* 49.2 (1994), p. 1473.

[21] Samuel L Braunstein and H Jeff Kimble. “Teleportation of continuous quantum variables”. In: *Physical Review Letters* 80.4 (1998), p. 869.

[22] Akira Furusawa et al. “Unconditional quantum teleportation”. In: *science* 282.5389 (1998), pp. 706–709.

[23] R.J.D Tilley. *Crystals and crystal structures*. Hoboken, NJ : John Wiley, 2006.

[24] XL Chen et al. “Negative refraction: an intrinsic property of uniaxial crystals”. In: *Physical Review B* 72.11 (2005), p. 113111.

[25] D. Eimerl et al. “Optical, mechanical, and thermal properties of barium borate”. In: *Journal of Applied Physics* 62.5 (1987), pp. 1968–1983. DOI: 10.1063/1.339536. eprint: https://doi.org/10.1063/1.339536. URL: https://doi.org/10.1063/1.339536.

[26] Gorachand Ghosh. “Dispersion-equation coefficients for the refractive index and birefringence of calcite and quartz crystals”. In: *Optics Communications* 163.1 (1999), pp. 95–102. ISSN: 0030-4018. DOI: https://doi.org/10.1016/S0030-4018(99)00091-7. URL: https://www.sciencedirect.com/science/article/pii/S0030401899000917.

[27] Rubén A. Fritz, Yamil J. Colón, and Felipe Herrera. “Engineering entangled photon pairs with metal–organic frameworks”. In: *Chem. Sci.* 12 (10 2021), pp. 3475–3482. DOI: 10.1039/D0SC05572G. URL: http://dx.doi.org/10.1039/D0SC05572G.

[28] Colin R Groom et al. “The Cambridge structural database”. In: *Acta Crystallographica Section B: Structural Science, Crystal Engineering and Materials* 72.2 (2016), pp. 171–179.

[29] Peyman Z Moghadam et al. “Development of a Cambridge Structural Database subset: a collection of metal–organic frameworks for past, present, and future”. In: *Chemistry of Materials* 29.7 (2017), pp. 2618–2625.

[30] Stijn Van Cleuvenbergen et al. “ZIF-8 as nonlinear optical material: influence of structure and synthesis”. In: *Chemistry of Materials* 28.9 (2016), pp. 3203–3209.

[31] Zhihui Chen et al. “Giant Enhancement of Second Harmonic Generation Accompanied by the Structural Transformation of 7-Fold to 8-Fold Interpenetrated Metal–Organic Frameworks (MOFs)”. In: *Angewandte Chemie International Edition* 59.2 (2020), pp. 833–838.

[32] Bo Xiao et al. “Chemically blockable transformation and ultraselective low-pressure gas adsorption in a non-porous metal organic framework”. In: *Nature chemistry* 1.4 (2009), pp. 289–294.

[33] Michelle H Teplensky et al. “A highly porous metal-organic framework system to deliver payloads for gene knockdown”. In: *Chem* 5.11 (2019), pp. 2926–2941.

[34] Javier Enríquez et al. “Controlled Growth of the Noncentrosymmetric Zn(3-ptz)2 and Zn(OH)(3-ptz) Metal–Organic Frameworks”. In: *ACS Omega* 4.4 (2019), pp. 7411–7419. DOI: 10.1021/acsomega.9b00236. eprint: https://doi.org/10.1021/acsomega.9b00236. URL: https://doi.org/10.1021/acsomega.9b00236.

[35] Dik Bouwmeester et al. “Experimental quantum teleportation”. In: *Nature* 390.6660 (Dec. 1997), pp. 575–579. ISSN: 1476-4687. DOI: 10.1038/37539. URL: https://doi.org/10.1038/37539.

[36] P. Walther et al. “Experimental one-way quantum computing”. In: *Nature* 434.7030 (Mar. 2005), pp. 169–176. ISSN: 1476-4687. DOI: 10.1038/nature03347. URL: https://doi.org/10.1038/nature03347.

[37] Wolfgang Tittel and Gregor Weihs. “Photonic Entanglement for Fundamental Tests and Quantum Communication”. In: *arXiv e-prints*, quant-ph/0107156 (July 2001), quant–ph/0107156. arXiv: quant-ph/0107156 [quant-ph].

[38] William TM Irvine. *Single photons in nonlinear photonic crystals and studies on electromagnetic knots*. University of California, Santa Barbara, 2006.

[39] Wolfgang Tittel et al. “Quantum cryptography using entangled photons in energy-time Bell states”. In: *Physical review letters* 84.20 (2000), p. 4737.

[40] Eric Dauler et al. “Tests of a two-photon technique for measuring polarization mode dispersion with subfemtosecond precision”. In: *Journal of research of the National Institute of Standards and Technology* 104.1 (1999), p. 1.

[41] Todd B Pittman et al. “Optical imaging by means of two-photon quantum entanglement”. In: *Physical Review A* 52.5 (1995), R3429.

[42] Mackillo Kira et al. “Quantum spectroscopy with Schrödinger-cat states”. In: *Nature Physics* 7.10 (2011), pp. 799–804.

[43] Agedi N Boto et al. “Quantum interferometric optical lithography: exploiting entanglement to beat the diffraction limit”. In: *Physical Review Letters* 85.13 (2000), p. 2733.

[44] Fabian Steinlechner et al. “Efficient heralding of polarization-entangled photons from type-0 and type-II spontaneous parametric downconversion in periodically poled KTiOPO 4”. In: *JOSA B* 31.9 (2014), pp. 2068–2076.

[45] Yanhua Shih. “Entangled biphoton source-property and preparation”. In: *Reports on Progress in Physics* 66.6 (2003), p. 1009.

[46] James Schneeloch et al. In: *Journal of Optics* 21.4 (2019), p. 043501.

[47] James Schneeloch et al. “Introduction to the absolute brightness and number statistics in spontaneous parametric down-conversion”. In: *Journal of Optics* 21.4 (2019), p. 043501.